PHYSICAL REVIEW B **96**, 060402(R) (2017)

Longitudinal spin Seebeck effect in a half-metallic $La_{0.7}Sr_{0.3}MnO_3$ film

B. W. Wu,[1] G. Y. Luo,[1,2] J. G. Lin,[2] and S. Y. Huang[1,*]

[1]*Department of Physics, National Taiwan University, Taipei, 10617, Taiwan*

[2]*Center for Condensed Matter Sciences, National Taiwan University, Taipei, 10617, Taiwan*

(Received 2 April 2017; revised manuscript received 13 May 2017; published 2 August 2017)

The longitudinal spin Seebeck effect (LSSE) with a vertical temperature gradient is one of the most important mechanisms to generate pure spin current. Previous studies of the LSSE excited spin current focus mainly on the magnetic insulators, a little on ferromagnetic metals, and rarely on ferromagnetic half metals. In this work, we demonstrate a significant spin current injected from the highly spin polarized ferromagnetic half metal $La_{0.7}Sr_{0.3}MnO_3$ by the LSSE. The sign of the thermal voltage can be reversed by using the spin current detector Cr with a large negative spin Hall angle. The ratio of the inverse spin Hall voltage to the total thermal signal in $La_{0.7}Sr_{0.3}MnO_3$ is much larger than that in ferromagnetic metals, such as permalloy and CoFeB. The nontrivial temperature-dependent voltage suggests that the thermal transport in $La_{0.7}Sr_{0.3}MnO_3$ is carried by magnons. This study provides insight into the mechanism of thermally excited spin current in ferromagnetic half metals and recommends the highly spin polarized $La_{0.7}Sr_{0.3}MnO_3$ as a promising candidate for metal-based spin caloritronics devices.

DOI: 10.1103/PhysRevB.96.060402

The manipulation of pure spin current for the development of novel spintronic devices has drawn much attention but remains a challenge. The spin Seebeck effect (SSE) is one of the most important mechanisms to drive the pure spin current by a thermal gradient. Based on the measurement geometry, the SSE can be classified into the transverse spin Seebeck effect (TSSE) with the in-plane temperature gradient and the longitudinal spin Seebeck effect (LSSE) with the out-of-plane temperature gradient [1,2]. They both require a heterostructure consisting of a thin normal-metal (NM) layer as a spin current detector and a magnetic material as a spin current generator which could be a conductor or insulator. By applying a temperature gradient, the heat current drives the pure spin current with spin angular momentum from the magnetic material into the NM. Subsequently, the pure spin current can be converted into the charge current and be electrically detected in the NM through the strong spin-orbit coupling with the inverse spin Hall effect (ISHE) [3,4]. Although the SSE in magnetic insulators, including ferrimagnetic and antiferromagnetic insulators, has been extensively studied, the SSE experiments in ferromagnetic metals (FMs) have not been conclusively established [2,5–7], mainly because the TSSE signal from FMs can easily be contaminated by the anomalous Nernst effect (ANE) due to an unintentional vertical temperature gradient and also because the LSSE signal is often overwhelmed by the preeminent ANE [8–10]. Therefore, it remains a challenge to generate the pure spin current from the FMs by the SSE.

Since the thermal spin transport is strongly correlated to the spin-dependent Seebeck coefficient of the FM, the generation efficiency of the pure spin current may be enhanced if the spin-up and spin-down electrons at the Fermi level have a large difference in the density of states [11,12]. Therefore, we aim to study the thermal generation of pure spin current in the ferromagnetic half metal $La_{0.7}Sr_{0.3}MnO_3$ (LSMO) with a high spin polarization in the 3*d* band [13,14]. Previously, Bui and Rivadulla reported on the thermal voltage of Pt/LSMO and attributed it to the planar and anomalous Nernst effects [15]. But Shiomi *et al.* suggested that the SSE may play an important role in the thermal signal of LSMO/$SrRuO_3$ superlattices [16]. Despite the different experimental conclusions, there is consensus that the perovskite structure of LSMO with a high Curie temperature has a rich variety of electronic and magnetic properties, including high spin polarization, colossal magnetoresistance (CMR), charge/orbital ordering, phase separation, and soft coercivity [17]. In this work, with the LSSE measurement of high-quality epitaxial LSMO films, we provide unequivocal evidence for an intrinsic LSSE signal from LSMO. For comparison, we also study the LSSE on other ferromagnetic alloys, including permalloy $Ni_{80}Fe_{20}$ (Py) and $Co_{60}Fe_{20}B_{20}$ (CFB). We show that the LSSE drives a considerable electrical signal in Pt/LSMO, in contrast to the negligible LSSE signal in Pt/Py and Pt/CFB bilayer samples. Furthermore, it is found that the spin current detector Cr with a large negative spin Hall angle induces a sign reversal of ISHE voltage in Cr/LSMO but not in Cr/Py and Cr/CFB. We further perform the temperature T-dependent measurements to investigate the mechanism of the LSSE in Pt/LSMO. The nonmonotonic temperature-dependent ISHE voltage suggests the mechanism of LSSE excited spin current in LSMO is magnon mediated.

Epitaxial LSMO films with a thickness of 100 nm were grown at 800 °C by pulsed laser deposition (PLD) on the $SrTiO_3$ (001) substrate with 100 mTorr oxygen pressure, followed by *in situ* annealing at 400 °C in the atmospheric oxygen pressure. The crystal structures of films were characterized by X-ray diffraction (XRD) and tunneling electron microscopy (TEM). Figure 1(a) is the cross-section TEM image of a Pt/LSMO film, with the inset showing the electron diffraction pattern of LSMO. The clear interface boundary in Pt/LSMO and the bright diffraction spots in LSMO suggest good crystallinity of LSMO film. Figure 1(b) shows the θ-2θ XRD diffraction pattern, indicating a *c*-oriented film direction. It is noted that there is a small lattice mismatch (∼1%) between LSMO and $SrTiO_3$ (STO) [18]. The magnetic

*syhuang@phys.ntu.edu.tw

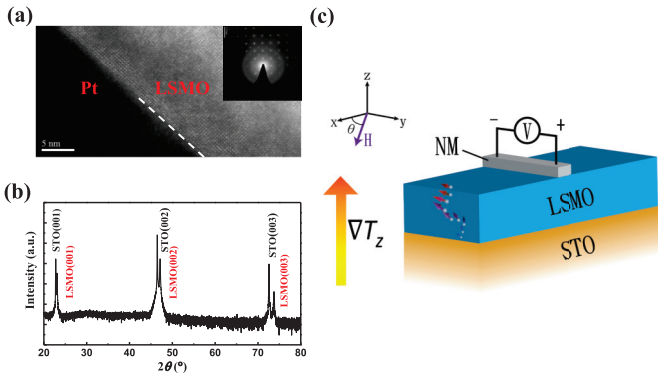

FIG. 1. (a) An overview cross-sectional TEM image for the Pt/LSMO sample. (b) X-ray diffraction pattern of LSMO/STO(001). (c) Schematic diagram of the longitudinal spin Seebeck effect for the spin injection with a vertical temperature gradient and the voltage measurement with the inverse spin Hall effect.

properties were investigated with a superconducting quantum interference device and vibrating sample magnetometers. The resistivity and magnetoresistance were measured using the four-probe method. The normal metals (Pt, W, and Cr) as well as the ferromagnetic metals (Py and CFB) were deposited with the magnetron sputtering. To obtain a systematic analysis, all FM layers were fixed as 100 nm. To have the optimal intensity of the ISHE signal, the NM layer varied from 3 to 5 nm, which is slightly larger than the spin diffusion length [19,20]. The large resistivity (160 μΩ cm) of W(5) could be a signature of the β-W phase [21,22]. The width of the NM is 3 mm, and the length is 5 mm. In order to have well-defined thermal transport directions, the LSSE geometry is used in this work to excite the heat current with a uniform out-of-plane (so-called vertical) temperature gradient which is controlled by a heater and a copper block heat sink [23,24]. To reduce systematic errors, we use constant power with the same heat flux density instead of a constant temperature difference to conduct the measurement [7,25,26]. The temperature gradient is measured with typical thermocouples and double-checked with the temperature dependence of resistance in the Pt layer [27]. An external in-plane magnetic field H is used to align the magnetization of LSMO along the x axis, as shown in Fig. 1(c). The configuration of the ANE voltage measurement without NM is the same as that of the ISHE voltage.

Figure 2(a) shows the T dependences of zero-field-cooled magnetization M and electrical resistivity for the single-layer LSMO film. The Curie temperature T_c is 355 K (i.e., the paramagnetic-to-ferromagnetic transition), consistent with that of bulk LSMO [28]. The resistivity decreases with decreasing T, confirming a metallic state below 350 K. The obtained high residual resistance ratio of 13 also implies a highly ordered conduction channel from the high-quality film. In Fig. 2(b), the room-temperature $M(H)$ curve of LSMO shows a soft ferromagnetic nature with a low coercivity field of 7 Oe. The shape anisotropy of the film can be calculated as $4\pi M_s = 5$ kOe, where M_s is the saturation magnetization.

The angle-dependent magnetoresistance (MR) at 750 Oe for Pt(3)/LSMO is shown in Fig. 2(c), where the number in parentheses is the layer thicknesses in nanometers. The MR behavior of Pt(3)/LSMO shows a typical twofold symmetry

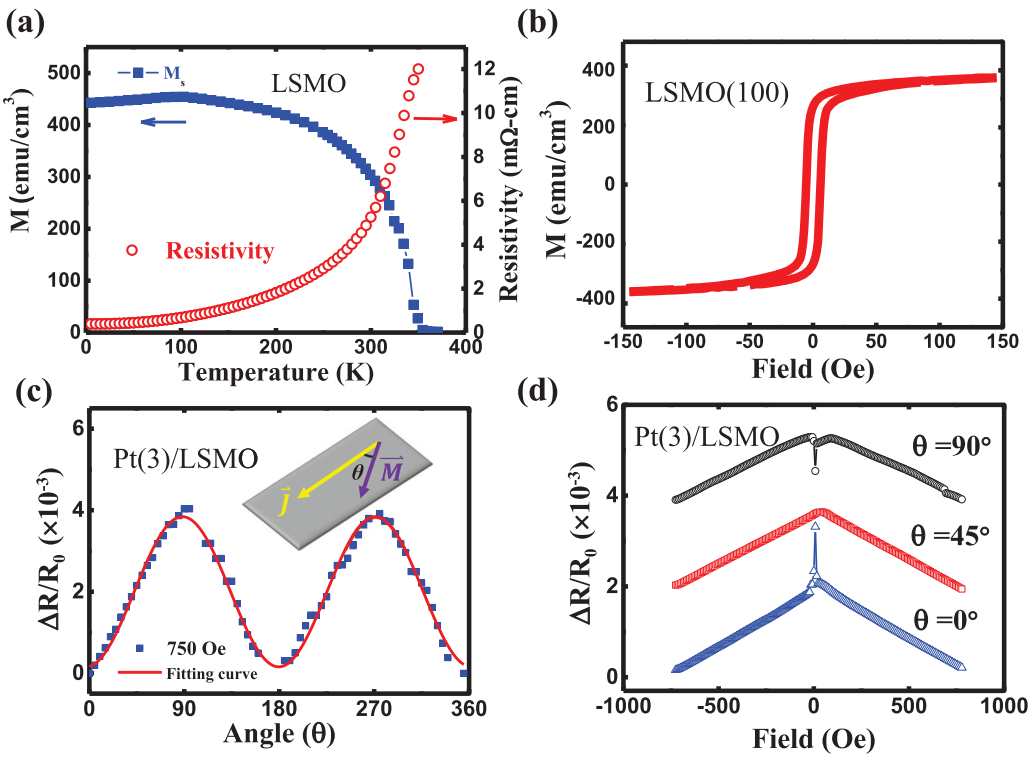

FIG. 2. (a) Temperature dependences of the magnetization under the condition of zero field cooling and the resistivity for the LSMO film. (b) The magnetic hysteresis loop of LSMO at room temperature. (c) Angular dependence of the anisotropy magnetoresistance and (d) field dependence of anisotropy magnetoresistance for the Pt(3)/LSMO sample at room temperature.

for a LSMO crystal, associated with the anisotropic MR effect. The MR ratio is defined as

$$\Delta R/R_{\parallel}(H) = [R_{\perp}(H) - R_{\parallel}(H)]/R_{\parallel}(H), \quad (1)$$

where $R_{\perp}(H)$ and $R_{\parallel}(H)$ are resistances with the magnetic field H being perpendicular and parallel to the electrical current, respectively. For comparison, the MR ratio is normalized by the resistivity at high field, $R_0 = R_{\parallel}(750\,\text{Oe})$. Here, $R_{\perp}(H) > R_{\parallel}(H)$ is opposite those observed in conventional polycrystalline ferromagnetic films, such as Fe, Co, and Ni [29]. The field-dependent MR in Fig. 2(d) shows a linear behavior due to the CMR effect [30,31].

In principle, the transverse thermal voltage could come from the ISHE with pure spin current and/or the ANE with spin-polarized current. The ISHE voltage can be described by

$$\boldsymbol{E}_{\text{ISHE}} \propto \theta_{\text{SH}} \boldsymbol{J}_{\text{S}} \times \boldsymbol{\sigma}, \quad (2)$$

where $\boldsymbol{E}_{\text{ISHE}}$ is the electric field produced by the ISHE, $\boldsymbol{J}_{\text{S}}$ is the spin current thrown into the NM, and $\boldsymbol{\sigma}$ is the spin-polarization vector. θ_{SH} is the spin Hall angle, which refers to the conversion efficiency of spin current to charge current. Since the conduction electrons of LSMO are polarized with unequal numbers of electrons of opposite spins, the spin-polarized current can also be generated in the transverse direction by the ANE when a vertical temperature gradient is unavoidably applied. Accordingly, the ANE voltage has the same magnetic field dependence as the ISHE [32–35]:

$$\boldsymbol{E}_{\text{ANE}} = \theta_{\text{ANE}} S_{xx} \hat{\boldsymbol{m}} \times \nabla \boldsymbol{T}, \quad (3)$$

where $\boldsymbol{E}_{\text{ANE}}$ is the electric field produced by the ANE, θ_{ANE} is the anomalous Nernst angle, S_{xx} is the Seebeck coefficient, and $\hat{\boldsymbol{m}}$ is the unit vector of magnetization. Thus, one needs to measure the ANE signal before analyzing the LSSE. As shown in Fig. 3(a), there is a significant ANE signal with asymmetric magnetic field dependence for the bare LSMO film at 275 K (see the open triangles). Here, the thermal voltage V_{th} is normalized by the vertical temperature gradient ∇T and the length of the sample along the y direction L_{y} as $\nabla V_{\text{th}}/\nabla T = (V_{\text{th}}/L_{\text{y}})/(\Delta T_{\text{z}}/t)$. The hysteresis loop of $\nabla V_{\text{th}}/\nabla T$ corresponds to the $M(H)$ loop, as expected from Eq. (3). Above 275 K, the signal is too small to measure within our experimental resolution (∼10 nV), which may be due to the abrupt reduction of M close to T_{c}, as shown in Fig. 2(a).

As shown in Fig. 3(a), the thermal voltage of the Pt(3)/LSMO bilayer sample is one order of magnitude larger than that of the bare LSMO. If the Pt layer merely serves as a shunting layer, the intensity of the signal should be reduced in Pt(3)/LSMO. Therefore, the significant enhancement of the thermal voltage in Pt(3)/LSMO is evidence of the LSSE excited ISHE voltage. We also normalize the thermal signal by the heat flux through the cross-section area of the sample. The scaling of the thermal voltage in Pt(3)/LSMO in terms of heat flux is estimated to be around 1.35×10^{-8} V m/W, which is comparable to but 8 times smaller than that of 1.1×10^{-7} V m/W in Pt(3)/YIG(60) [25]. The signal is further reduced by half when the Pt thickness is increased from 3 to 5 nm, reflecting the nature of the short spin diffusion length of Pt in Fig. 3(b) [19,36].

To provide additional evidence of the LSSE in LSMO, Pt is replaced by W and Cr as the probing layer with negative θ_{SH}. As shown in Fig. 3(b), the ISHE voltage of the W(5)/LSMO is not large enough to overcome the ANE, but that of Cr(3)/LSMO completely reverses the sign of $\nabla V_{\text{th}}/\nabla T$. The small LSSE in W(5)/LSMO is unusual since W has a significant spin-orbit coupling. However, Du *et al.* demonstrated that Cr and Ni showed a very large spin Hall angle, indicating that d-orbital filling rather than atomic number plays a dominant role in the spin Hall effect [37]. The magnitude of V_{ISHE} in Cr/LSMO is clearly larger than that of V_{ANE} in LSMO but with opposite sign, in agreement with the recent report on Cr/YIG. The 3d metal Cr has a large spin Hall angle which is even superior to that of 5d metals [19,20,37]. Since Cr has a low atomic number, we consider that the contribution of the proximity-induced ANE is negligibly small [38–40]. Thus, it is unambiguously demonstrated that the thermal voltage in the ferromagnetic half-metal LSMO is from intrinsic LSSE.

For comparison, the LSSE in other conventional ferromagnetic alloys is also investigated, including Py and CFB. Within different ferromagnetic metal systems, the sample dependences of resistivity and shunting effect have to be taken into account. A parallel circuit model allows us to normalize the measured thermal voltage V_{th} with the resistance of a different layer, as described by [41]

$$V_{\text{th}}/R_{\text{total}} = V_{\text{ANE}}/R_{\text{FM}} + V_{\text{ISHE}}/R_{\text{NM}}, \quad (4)$$

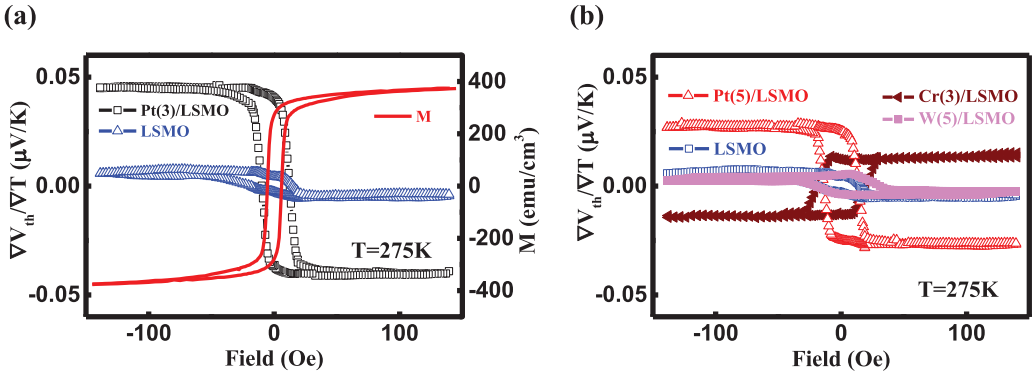

FIG. 3. (a) Magnetic field dependence of the thermal voltage for LSMO and Pt(3)/LSMO under a vertical temperature gradient of 6 K/mm (left y scale) and the $M(H)$ curve for LSMO (right y scale). (b) Magnetic field dependences of the thermal voltage for single-layer LSMO and bilayers NM/LSMO with NM = Pt(5), W(5), and Cr(3).

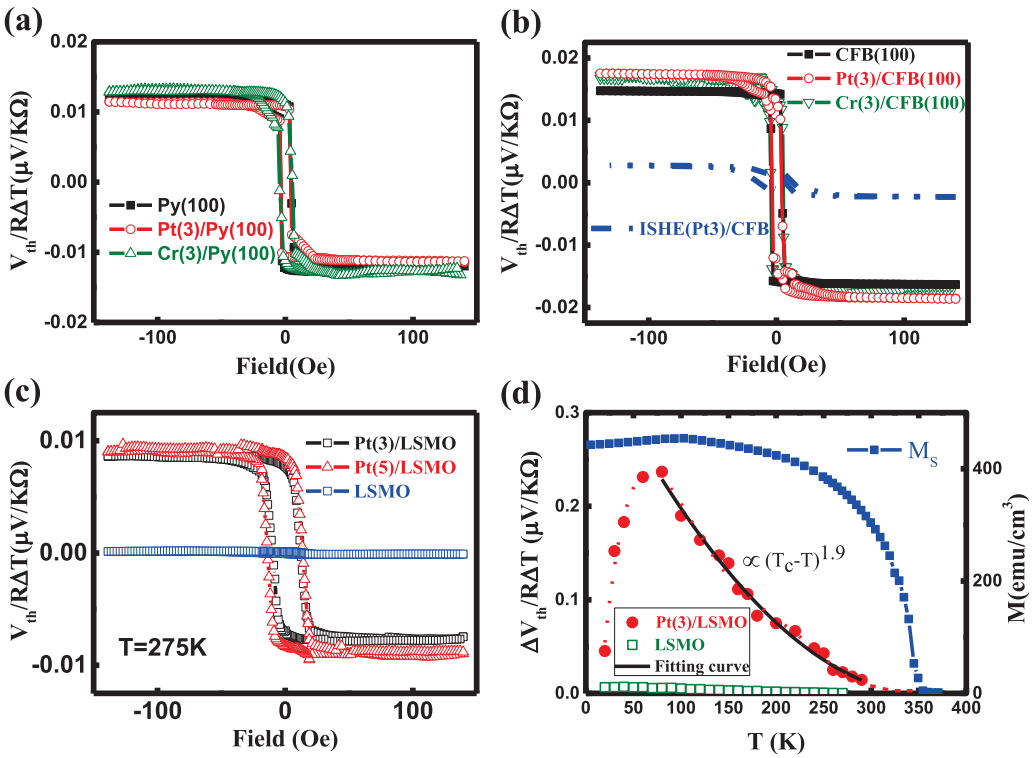

FIG. 4. Normalized thermal voltage of (a) Py, Pt(3)/Py, and Cr(3)/Py; (b) CFB, Pt(3)/CFB, and Cr(3)/CFB; and (c) LSMO, Pt(3)/LSMO, and Pt(5)/LSMO. (d) Temperature dependences of the magnetization for LSMO (right y scale) and the normalized thermal voltage for LSMO and Pt(3)/LSMO (left y scale). The black solid line is fitted by a power law with $\Delta V_{\rm th}/R\Delta T \propto (T_{\rm c}-T)^{\gamma}$. The R on the y axis represents the resistance of the NM/FM bilayer or that of the FM layer.

where $R_{\rm total}$, $R_{\rm FM}$, and $R_{\rm NM}$ are the resistances of the NM/FM bilayer, the FM, and the NM, respectively. As a consequence, one can separate the contribution of the ANE from the LSSE. In Fig. 4(a), the thermal voltages of Pt/Py and Cr/Py are almost equivalent to that of Py, suggesting $V_{\rm th}$ of three samples are dominated by the ANE voltage of Py. On the other hand, the thermal voltage of Pt(3)/CFB(100) may be composed of the LSSE and the ANE since it is slightly larger than that of CFB(100). After subtracting the ANE contribution, the ISHE voltage of Pt/CFB is shown as the blue dashed curve in Fig. 4(b). However, when the Cr with negative $\theta_{\rm SH}$ is used to detect the spin current from CFB, the signal cannot be reversed and is even slightly larger than the ANE signal of CFB in Fig. 4(b). Recently, a similar behavior was observed, and an additional ISHE voltage was attributed to the FM itself [41]. Overall, our results indicate the ANE dominates in both Py and CFB single layers. In sharp contrast, the origin of the thermal voltage in the half-metal LSMO layer is dominated by the ISHE from the LSSE with the ANE contribution being negligible. In addition, the normalized voltage curves of Pt(3)/LSMO and Pt(5)/LSMO almost overlap, confirming the validity of the parallel resistor model. The absolute anomalous Nernst angle $\theta_{\rm ANE}$, defined by the ratio of the anomalous Nernst voltage and Seebeck coefficient S_{xx} as $\theta_{\rm ANE} = E_{\rm ANE}/S_{xx}\nabla T$, is about 0.2% for Py and 1.2% for LSMO [15,42]. One can estimate the contribution of the ISHE in the total thermal signal by the ratio of $(\frac{V_{\rm ISHE}}{R_{\rm N}})/(\frac{V_{\rm th}}{R_{\rm total}})$. The upper bound of the ISHE in Pt/CFB is around 15%, and that in Pt/Py is negligibly small, while the contribution of the ISHE in Pt/LSMO is more than 95%. We suggest the transverse thermopower could be further enhanced by superimposing the SSE on the ANE in the form of multilayer or granular structures [2,43,44].

In order to explore the mechanism of the LSSE in LSMO, the T dependence of the LSSE is measured from 20 to 340 K. As shown in Fig. 4(d), $V_{\rm th}/(R\Delta T)$ of Pt/LSMO increases with decreasing T and has a sharp drop at ~80 K. The strong T dependence with a local maximum is similar to that in Pt/YIG [20,45], implying that these two systems share a common mechanism of thermal spin injection. The nonmonotonic T-dependent behavior is attributed to the change in the thermal magnon population. Accordingly, the competition between the magnon population and the lifetime of the magnon results in the peak around 80 K. In addition, near the Curie temperature (~350 K), the T dependence of the ISHE voltage in Pt/LSMO is very different from the $M(T)$ curve of LSMO, as shown in Fig. 4(d). A rapid decrease in the LSSE signal for $T > 80$ K can be fitted with a critical exponent of around 1.9 in the equation $\Delta V_{\rm th}/R\Delta T \propto (T_{\rm c}-T)^{1.9}$ [46]. The fact that this monotonic decrease in the ISHE voltage with increasing T reaches zero near $T_{\rm c}$ implies a reduction of the spin-mixing conductance, caused by the reduction of magnetization in LSMO, based on the magnon spin current model [46,47]. Therefore, it is very likely that the LSSE in the half-metallic LSMO is associated with the magnon excited spin current, having the same mechanism as that in magnetic insulators. Note that the LSSE has also been observed in ferrimagnetic Fe_3O_4 with half-metallic character [43,48], in which the magnon may generate spin current efficiently [49].

In summary, under a vertical temperature gradient, we conclusively demonstrated the LSSE in the ferromagnetic half-metal LSMO film. The sign of the thermal voltage can be reversed by using the spin current detector Cr with a negative spin Hall angle. Unlike Py and CFB in which the ANE dominates the transverse thermal transport, more than 95% of the thermal voltage comes from the LSSE in LSMO. The nontrivial behavior of the temperature dependence of the LSSE voltage reveals that the mechanism of the LSSE in LSMO is related to the magnon excitation. This study provides important insight into the origin of thermally driven pure spin current in ferromagnetic half metals and explores the possible applications of LSMO in spin caloritronics.

The authors would like to thank Prof. J. H. Hsu of National Taiwan University for the experimental support. This work was supported by the Ministry of Science and Technology of Taiwan under Grants No. MOST 103-2212-M-002-021-MY3 and No. MOST 105-2112-M-002-010-MY3. S.Y.H. acknowledges the Golden Jade Fellowship of the Kenda Foundation, Taiwan.

[1] G. E. Bauer, E. Saitoh, and B. J. van Wees, Nat. Mater. **11**, 391 (2012).
[2] K. Uchida, H. Adachi, T. Kikkawa, A. Kirihara, M. Ishida, S. Yorozu, S. Maekawa, and E. Saitoh, Proc. IEEE **104**, 1946 (2016).
[3] E. Saitoh, M. Ueda, H. Miyajima, and G. Tatara, Appl. Phys. Lett. **88**, 182509 (2006).
[4] A. Hoffmann, IEEE Trans. Magn. **49**, 5172 (2013).
[5] K.-D. Lee, D.-J. Kim, H. Yeon Lee, S.-H. Kim, J.-H. Lee, K.-M. Lee, J.-R. Jeong, K.-S. Lee, H.-S. Song, J.-W. Sohn *et al.*, Sci. Rep. **5**, 10249 (2015).
[6] S. Seki, T. Ideue, M. Kubota, Y. Kozuka, R. Takagi, M. Nakamura, Y. Kaneko, M. Kawasaki, and Y. Tokura, Phys. Rev. Lett. **115**, 266601 (2015).
[7] S. M. Wu, W. Zhang, Amit KC, P. Borisov, J. E. Pearson, J. S. Jiang, D. Lederman, A. Hoffmann, and A. Bhattacharya, Phys. Rev. Lett. **116**, 097204 (2016).
[8] S. Y. Huang, W. G. Wang, S. F. Lee, J. Kwo, and C. L. Chien, Phys. Rev. Lett. **107**, 216604 (2011).
[9] D. Meier, D. Reinhardt, M. van Straaten, C. Klewe, M. Althammer, M. Schreier, S. T. B. Goennenwein, A. Gupta, M. Schmid, C. H. Back, J.-M. Schmalhorst, T. Kuschel, and G. Reiss, Nat. Commun. **6**, 8211 (2015).
[10] J. Holanda, O. Alves Santos, R. O. Cunha, J. B. S. Mendes, R. L. Rodríguez-Suárez, A. Azevedo, and S. M. Rezende, Phys. Rev. B **95**, 214421 (2017).
[11] N. F. Mott and E. A. Davis, *Electronic Processes in Non-crystalline Materials* (Clarendon Press, Oxford, 1979).
[12] S. Hu, H. Itoh, and T. Kimura, NPG Asia Mater. **6**, e127 (2014).
[13] J. H. Park, E. Vescovo, H. J. Kim, C. Kwon, R. Ramesh, and T. Venkatesan, Nature (London) **392**, 794 (1998).
[14] M. Bowen, M. Bibes, A. Barthelemy, J.-P. Contour, A. Anane, Y. Lemaitre, and A. Fert, Appl. Phys. Lett. **82**, 233 (2003).
[15] C. T. Bui and F. Rivadulla, Phys. Rev. B **90**, 100403(R) (2014).
[16] Y. Shiomi, Y. Handa, T. Kikkawa, and E. Saitoh, Appl. Phys. Lett. **106**, 232403 (2015).
[17] S. Majumdar and S. van Dijken, J. Phys. D **47**, 034010 (2014).
[18] G. Y. Luo, M. Belmeguenai, Y. Roussigné, C. R. Chang, J. G. Lin, and S. M. Chérif, AIP Adv. **5**, 097148 (2015).
[19] D. Qu, S. Y. Huang, B. F. Miao, S. X. Huang, and C. L. Chien, Phys. Rev. B **89**, 140407(R) (2014).
[20] D. Qu, S. Y. Huang, and C. L. Chien, Phys. Rev. B **92**, 020418(R) (2015).
[21] C.-F. Pai, L. Liu, Y. Li, H. W. Tseng, D. C. Ralph, and R. A. Buhrman, Appl. Phys. Lett. **101**, 122404 (2012).
[22] Q. Hao, W. Chen, and G. Xiao, Appl. Phys. Lett. **106**, 182403 (2015).
[23] P. H. Wu and S. Y. Huang, Phys. Rev. B **94**, 024405 (2016).
[24] Y. J. Chen and S. Y. Huang, Phys. Rev. Lett. **117**, 247201 (2016).
[25] A. Sola, P. Bougiatioti, M. Kuepferling, D. Meier, G. Reiss, M. Pasquale, T. Kuschel, and V. Basso, Sci. Rep. **7**, 46752 (2017).
[26] S. M. Wu, F. Y. Fradin, J. Hoffman, A. Hoffmann, and A. Bhattacharya, J. Appl. Phys. **117**, 17C509 (2015).
[27] K.-i. Uchida, T. Kikkawa, A. Miura, J. Shiomi, and E. Saitoh, Phys. Rev. X **4**, 041023 (2014).
[28] J. M. D. Coey, M. Viret, L. Ranno, and K. Ounadjela, Phys. Rev. Lett. **75**, 3910 (1995).
[29] S. Kokado and M. Tsunoda, Adv. Mater. Res. **750-752**, 978 (2013).
[30] Y. Lu, X. W. Li, G. Q. Gong, G. Xiao, A. Gupta, P. Lecoeur, J. Z. Sun, Y. Y. Wang, and V. P. Dravid, Phys. Rev. B **54**, R8357 (1996).
[31] Y. Bason, L. Klein, J.-B. Yau, X. Hong, and C. H. Ahn, Appl. Phys. Lett. **84**, 2593 (2004).
[32] A. Slachter, F. L. Bakker, and B. J. van Wees, Phys. Rev. B **84**, 020412(R) (2011).
[33] M. Mizuguchi, S. Ohata, K. Uchida, E. Saitoh, and K. Takanashi, Appl. Phys. Express **5**, 093002 (2012).
[34] S. J. Watzman, R. A. Duine, Y. Tserkovnyak, S. R. Boona, H. Jin, A. Prakash, Y. Zheng, and J. P. Heremans, Phys. Rev. B **94**, 144407 (2016).
[35] X. Li, L. Xu, L. Ding, J. Wang, M. Shen, X. Lu, Z. Zhu, and K. Behnia, Phys. Rev. Lett. (to be published).
[36] M. Isasa, E. Villamor, L. E. Hueso, M. Gradhand, and F. Casanova, Phys. Rev. B **91**, 024402 (2015).
[37] C. H. Du, H. L. Wang, F. Y. Yang, and P. C. Hammel, Phys. Rev. B **90**, 140407(R) (2014).
[38] S. Y. Huang, X. Fan, D. Qu, Y. P. Chen, W. G. Wang, J. Wu, T. Y. Chen, J. Q. Xiao, and C. L. Chien, Phys. Rev. Lett. **109**, 107204 (2012).
[39] T. Kikkawa, K. Uchida, S. Daimon, Y. Shiomi, H. Adachi, Z. Qiu, D. Hou, X.-F. Jin, S. Maekawa, and E. Saitoh, Phys. Rev. B **88**, 214403 (2013).
[40] B. F. Miao, S. Y. Huang, D. Qu, and C. L. Chien, AIP Adv. **6**, 015018 (2016).
[41] Y. Xu, B. Yan, C. Tang, Z. Jiang, M. Schneider, R. Whig, and J. Shi, Appl. Phys. Lett. **105**, 242404 (2014).

[42] K. Uchida, S. Takahashi, K. Harii, J. Ieda, W. Koshibae, K. Ando, S. Maekawa, and E. Saitoh, Nature (London) **455**, 778 (2008).

[43] R. Ramos, T. Kikkawa, M. H. Aguirre, I. Lucas, A. Anadón, T. Oyake, K. Uchida, H. Adachi, J. Shiomi, P. A. Algarabel, L. Morellón, S. Maekawa, E. Saitoh, and M. R. Ibarra, Phys. Rev. B **92**, 220407(R) (2015).

[44] S. R. Boona, K. Vandaele, I. N. Boona, D. W. McComb, and J. P. Heremans, Nat. Commun. **7**, 13714 (2016).

[45] A. Prakash, B. Flebus, J. Brangham, F. Yang, Y. Tserkovnyak, and J. P. Heremans, arXiv:1706.09021.

[46] S. M. Rezende, R. L. Rodríguez-Suárez, R. O. Cunha, A. R. Rodrigues, F. L. A. Machado, G. A. Fonseca Guerra, J. C. Lopez Ortiz, and A. Azevedo, Phys. Rev. B **89**, 014416 (2014).

[47] S. Wang, L. Zou, X. Zhang, J. Cai, S. Wang, B. Shen, and J. Sun, Nanoscale **7**, 17812 (2015).

[48] R. Ramos, T. Kikkawa, K. Uchida, H. Adachi, I. Lucas, M. H. Aguirre, P. Algarabel, L. Morellon, S. Maekawa, E. Saitoh, and M. R. Ibarra, Appl. Phys. Lett. **102**, 072413 (2013).

[49] M. I. Katsnelson, V. Yu. Irkhin, L. Chioncel, A. I. Lichtenstein, and R. A. de Groot, Rev. Mod. Phys. **80**, 315 (2008).